

Impact of surface roughness temperature dependency on the thermal contact resistance between Si(111) and liquid ^4He

J. Amrit

LIMSI-CNRS, Université Paris-Sud 11, BP 133, F-91403 Orsay, France

(Received 20 February 2009; revised manuscript received 16 December 2009; published 8 February 2010)

The thermal contact resistance at a highly polished single-crystal silicon (111)/liquid helium interface has been directly measured from 0.4 to 2.1 K using a single experimental cell. A thermal analysis is presented using the thermal conductivity of the Si which is simultaneously measured. The effect of phonon scattering by nanoscale surface roughness on the observed thermal resistance is investigated. A feature brought to light in our analysis is that the surface roughness which plays an effective role in phonon scattering is temperature dependent. This explains the temperature dependencies of the thermal contact resistance. Comparisons with other experiments are made.

DOI: [10.1103/PhysRevB.81.054303](https://doi.org/10.1103/PhysRevB.81.054303)

PACS number(s): 72.10.Di, 68.08.-p, 67.80.bf

I. INTRODUCTION

The Kapitza thermal contact resistance (TCR) at solid/superfluid ^4He boundaries is probably one of the most puzzling thermal phenomena yet to be *quantitatively* understood. The thermal barrier ΔT , which is formed over just a few atomic layers at the interface, is typically two or more orders of magnitude greater than the temperature difference over 1 mm in the solid. The TCR is given by $\Delta T/(\dot{Q}/A_I)$, where \dot{Q} is the heat flow and A_I is the cross-sectional area of the interface. The considerable amount of theoretical and experimental work¹⁻³ at $T > 1$ K has led to the general consensus that there are two parallel channels of heat transfer: a weak channel determined by elastic properties of each medium in which phonons undergo specular reflection, described by the acoustic mismatch (AM) theory,⁴ and an important background channel in which, contrary to the former mechanism, the components of the wave vectors of phonons parallel to the surface are not conserved at the interface. Here, a single incident phonon on the surface can give rise to one or more phonons which are reflected and/or absorbed at the interface. This phenomenon is qualitatively attributed to surface nonideality⁵ which was studied theoretically.^{6,19}

We report here an experimental study which focuses on the impact of surface roughness on phonon transmission, based on the theory of Adamenko and Fuks (AF).⁷ In the AF theory the phonon momentum transfer is determined by the δ/λ ratio, where δ is the characteristic surface roughness dimension and $\lambda \approx \hbar c_L/3.8k_B T$ is the phonon wavelength in liquid He and c_L is the sound velocity in He. Our study is based on the premise that by changing the temperature the ratio δ/λ is modulated and hence the nature (diffuse or specular) of the phonon scattering can be experimentally “tuned” for a highly polished surface. Our experiment is conducted on a highly polished silicon [111] crystal surface in contact with superfluid ^4He from 0.4 to 2.1 K using a unique experimental cell. The mean roughness of the Si surface is less than 1 nm on scale length of ~ 1 μm . And, the thermal phonon wavelengths in liquid He vary from 8 to 2 nm in the experimental temperature range whereas in Si the wavelengths vary from 650 to 65 nm. The results demonstrate that the TCR is dominated by the phonon-surface roughness in-

teraction at the interface in the whole temperature range of the experiment. We show that the surface roughness height σ , required to quantitatively account for the experimental transmission coefficient, is nanometric in scale. Moreover, the surface roughness which comes into play depends on temperature and this in turn can explain successfully the temperature dependency of the TCR from 0.4 to 2.1 K.

This paper is organized as follows. We describe our experimental cell geometry. A heat flow analysis is presented to interpret and show the reliability of our measurements. The thermal conductivity of our Si single crystal is discussed. The direct measurements of the Kapitza resistance between Si(111) and superfluid ^4He under *svp* pressure from 0.4 K to the λ point are presented. The influence of the surface roughness on the temperature behavior of the average transmission coefficient is quantified in light of the AF model. Finally, our results are compared to other studies at Si/ ^4He boundaries.

II. EXPERIMENT

A. Cell configuration and sample

Our experimental arrangement is shown in Fig. 1. The silicon sample is a rod-shaped single crystal (6.2 mm in diameter and ~ 40 mm in length). It is of intrinsic purity and was supplied by Crystal Scientific® (UK) Limited. The crystal was Flotzone grown and its c axis is oriented long the (111) direction. The flat [111] plane in contact with superfluid helium is an optically polished silver mirrorlike surface. Its surface roughness characterization is described later (Sec. III). The other surfaces are grayish in color. The crystal was handled under He atmosphere, but it was exposed to air for few minutes when mounting the cell onto the refrigerator.

The experimental cell also consists of a thin walled CuNi tube (~ 0.15 mm wall thickness and ~ 38 mm in length) which is soldered to an ~ 1 cm^3 copper reservoir. At the other extremity of the tube, the silicon rod is sealed superfluid leak-tight over a length $l \approx 2.2$ mm into the tube, using a fine layer of Stycast 2852 FT. The mounting of the Si crystal rod is achieved as follows. A Teflon rod, of diameter equal to that of the CuNi tube, was tightly inserted through the copper reservoir along the length of the tube up to l

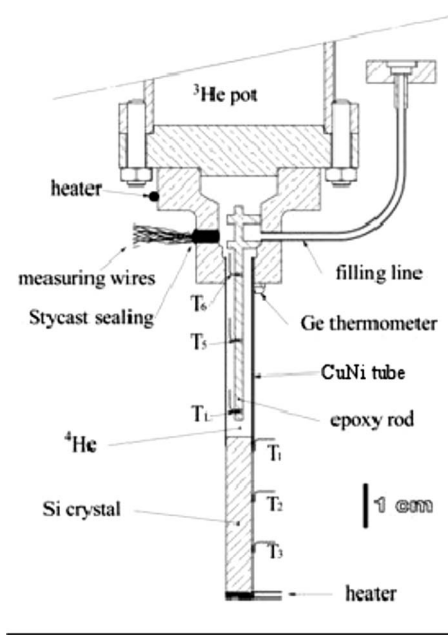


FIG. 1. Experimental cell.

≈ 2.2 mm from the other extremity of tube. The CuNi tube was inserted through the centre of a Teflon disk (of ~ 5 cm in diameter and ~ 3 cm in thickness). Similarly, the Si rod was inserted through the centre of a second Teflon disk of same dimensions. A fine layer of Stycast 2852 FT was applied carefully over a length of ~ 1.8 mm on the side walls of the crystal rod, which was then delicately inserted into the CuNi tube. The two Teflon disks were brought together at the crystal/tube junction and aligned with the aid of grooves (which were machined on them). This procedure helped to align the crystal axis to that of the tube. The Stycast seal over the length of $l \approx 2.2$ mm of the tube is achieved by the spreading of the Stycast during the insertion of the crystal and also by capillary effects since Stycast 2852 FT (with catalyst 24LV) is a low viscosity epoxy.⁸ The purpose of Teflon rod in the CuNi tube was threefold: to monitor the depth of the crystal into the rod, to protect the study sample surface of Stycast and to prevent the Stycast from creeping onto the CuNi tube wall beyond 2.2 mm. After ~ 50 h, the Teflon disks and rod were removed, and the sample surface was examined.

The copper reservoir is fixed to cold source of the ^3He refrigerator. The reservoir and the tube are filled with liquid helium at *svp* pressure.

We use bare chipped ruthenium oxide (Model RX-102A-BR) thermometers. They were calibrated together in a cell filled with superfluid helium. Three of these thermometers are fixed to the crystal with a fine layer of Araldite[®] glue. Three other RX thermometers are mounted onto an epoxy stick (~ 0.8 mm in diameter) which is suspended into the CuNi tube to measure the liquid temperature. The distance from the interface to the closet thermometer in the liquid T_L is ~ 2.5 mm. The distance from the interface to the centre of thermometer T_1 on the crystal is $d \approx 2.8$ mm. A Manganin wire heater ($\sim 64 \Omega$) is tightly wound to the extremity of the crystal over a length of ~ 5 mm and it supplies the phonon

flux which is conducted along the Si(111) direction and across the interface. A calibrated Ge thermometer (model GR-200A) and a carbon heater (560Ω) are anchored to the top of the cell; and they are used to control the liquid He temperature.

B. Measuring technique

During an experiment we record the temperature evolution along the crystal, indicated by T_1 , T_2 , and T_3 , and in liquid He (T_L) as a steady heating power is supplied to the crystal (see Fig. 1). The temperature on the liquid-side of the interface T_{LI} is held constant throughout an experiment. The evolution of T_1 is essentially governed by the reflection of phonons at the interface boundary and by the thermal conductivity of the Si crystal. Heat losses from the crystal to the CuNi tube over the length l also modifies T_1 . The temperature on the solid side of the interface is given by $T_{SI} = [T_1 - (d/K_{Si})\dot{Q}_I]$, where K_{Si} is the thermal conductivity of Si and \dot{Q}_I is the effective heat flux crossing the interface. Since the temperature on the liquid side T_{LI} is constant, a change in the heat flux $\Delta\dot{Q}_I$ across the interface produces a temperature change from T_1 to T'_1 , which is given by

$$A_l(T_1 - T'_1) = (R_K + d/K_{Si})\Delta\dot{Q}_I. \quad (1)$$

It is easily seen that the Kapitza resistance at the interface can now be expressed as follows:

$$R_K = (T_{SI} - T'_{SI})A_l/\Delta\dot{Q}_I. \quad (2)$$

III. RESULTS AND ANALYSIS

A typical set of data acquisition are shown in Fig. 2. The absolute error in the stability of the superfluid temperature T_L varies from 0.0125% at 0.4 K to 0.025% at 2.1 K. In Fig. 2 the thermal gradient in the Si crystal between thermometers T_1 and T_2 is ~ 0.25 mK/mm when $\dot{Q}_I \approx 40 \mu\text{W}$. For the same heat flux crossing the interface, the Kapitza temperature jump is ~ 25 mK over just a few atomic layers. The strong phonon reflection at the interface is clearly detected by all three thermometers on the crystal on a time scale which is given by $\tau \approx (x^2/D)$, where x is the distance between the interface and the thermometer and $D \approx 10^6 \text{ cm}^2/\text{s}$ is the thermal diffusivity in Si at low temperatures. This thermal diffusion time varies from $\sim 0.1 \mu\text{s}$ for T_1 to $\sim 50 \mu\text{s}$ for T_3 .

A. Thermal conductivity of silicon (111)

In our experimental geometry the thermal conductivity of the Si crystal along the (111) direction is also simultaneously determined from $K_{Si} = \dot{Q}_o/[A_l(dT/dx)]$, where \dot{Q}_o is the input heat. In calculating the gradient (dT/dx) we supposed that the Kapitza resistance between a thermometer and the crystal surface is identical for all the thermometers on the crystal. This may explain the small dispersion in our thermal conductivity results shown in Fig. 3.

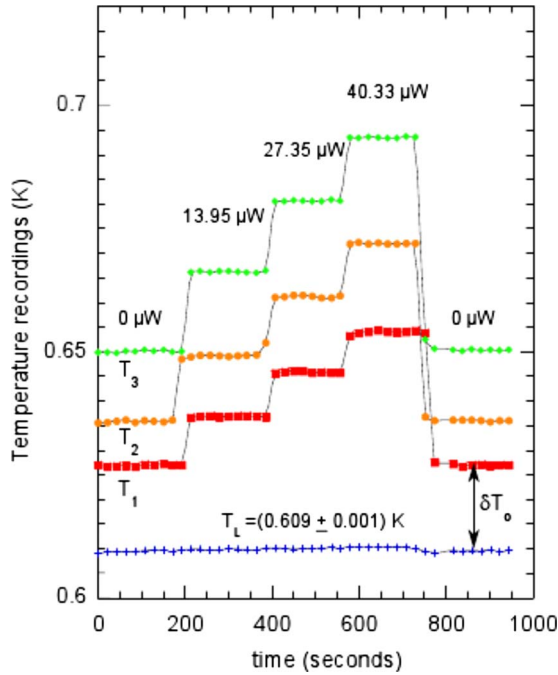


FIG. 2. (Color online) Typical temperature recording of thermometers T_1 , T_2 , and T_3 on the crystal and in liquid He T_L as a function of heating power. Data points are interpolated for clarity. The Kapitza temperature jumps are clearly observable as the liquid temperature remains controlled.

The dashed line fit to our data is calculated using $K_{Si} = \frac{1}{3}Cv_D\ell$, where the specific heat and the Debye sound velocity are, respectively,⁹ $C=6.02 \times 10^{-7}T^3$ ($J \text{ cm}^{-3} \text{ K}^{-1}$) and $v_D=5.93 \times 10^5$ cm/s. The average mean free path used in this fit has a constant value of $\ell=0.52$ cm. The fit corresponds to $K_{Si}=0.0619T^3$ ($W \text{ cm}^{-1} \text{ K}^{-1}$). The T^3 behavior is characteristic of diffuse scattering (Casimir) of phonons at

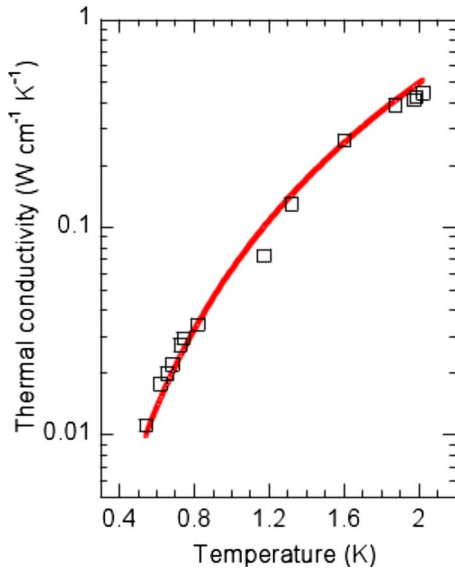


FIG. 3. (Color online) Thermal conductivity measurements (squares) along the $[111]$ axis of our single-crystal Si sample. An average mean free path of phonons $\ell=0.52$ cm is used to obtain the solid line fit which corresponds to $K(T)=0.0619T^3$ ($W \text{ cm}^{-1} \text{ K}^{-1}$).

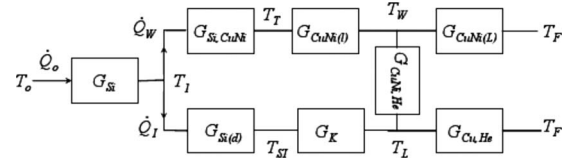


FIG. 4. Heat flow paths in the experimental cell.

the sample walls parallel to heat flow direction. There is also a very good agreement between our data and the measurements performed on Si(111) samples (pencil-shaped structures) by Klitsner and Pohl⁹ [$K_{KP}=0.057T^3$ ($W \text{ cm}^{-1} \text{ K}^{-1}$)].

With $d \approx 2.8$ mm we estimate that the influence of the thermal resistance d/K_{Si} in Eq. (1) is only $\sim 3\%$ at 2 K and $\sim 6\%$ at 0.4 K. Our average phonon mean free path ℓ determined above exceeds the length d of the crystal between the interface and T_1 . Consequently, the above d/K_{Si} estimate is an upper limit.

B. Thermal analysis of raw data

Up to now only the standard technique involving direct temperature measurements gives access to R_K as a function of T . Using this technique in a large temperature range imposes constraints on the experimental cell design mainly so because heat flow paths in a cell and thus, across the interface are modified with temperature, since Kapitza resistances in different parts of the cell change as well. This explains the lack of experimental data on well characterized solid surfaces in a large temperature range. To show the reliability of our experiment, we analyze our raw data with the aid of a thermal model represented in Fig. 4. To quantify heat flow we estimated the conductance along each of the different heat paths in the cell as follows. The input heat \dot{Q}_o is conducted along the c axis of the crystal of sectional area A_j . The conductance in the crystal between the heater and T_1 is given by $G_{Si}=(K_{Si}/L)=0.019T^3$ ($W \text{ cm}^{-2} \text{ K}^{-1}$). At the Si/CuNi tube junction, \dot{Q}_W is lost to the CuNi tube over an area of $A_{Si,CuNi} \propto l$. We took this conductance $G_{Si,CuNi}$ to be the Kapitza conductance between the Si crystal and the CuNi tube. To estimate $G_{Si,CuNi}$ we use the expression for a solid-solid interface,¹⁰ that is, $G_{Si,CuNi} = \frac{\pi^2 k_B^2 T}{120 \hbar^2} \left[\frac{\tilde{\alpha}_L}{c_L^2} + \frac{2\tilde{\alpha}_T}{c_T^2} \right] T^3$, where $\tilde{\alpha}_L = \frac{4z_{1L}z_{2L}}{(z_{1L}+z_{2L})^2}$ and $\tilde{\alpha}_T = \frac{4z_{1T}z_{2T}}{(z_{1T}+z_{2T})^2}$ are, respectively, the transmission coefficients of the longitudinal (L) and transverse (T). Here the acoustic impedance $z_{ij} = \rho_i c_j$, where ρ is the density, c is the sound velocity, $j=L, T$ and $i=1, 2$ refer, respectively, to medium 1 and 2. We computed $\tilde{\alpha}_L=0.853$ and $\tilde{\alpha}_T=0.896$ with the following values for Si (Ref. 9): $\rho_{Si}=2.33$ g/cm³, $c_L=8.97 \times 10^5$ cm/s, and $c_T=5.332 \times 10^5$ cm/s; for the CuNi tube we used:¹¹ $\rho_{CuNi}=8.89$ g/cm³, $c_L=5.98 \times 10^5$ cm/s, and $c_T=3.297 \times 10^5$ cm/s. The conductance came out to be $G_{Si,CuNi}=0.0188T^3$ ($W \text{ cm}^{-2} \text{ K}^{-1}$). Heat entering the CuNi wall is conducted over the length l up to the interface. The associated conductance is $G_{CuNi(l)}=(K_{CuNi}/l)=3.1 \times 10^{-3}T^3$ ($W \text{ cm}^{-2} \text{ K}^{-1}$), where $K_{CuNi}=9.3 \times 10^{-4}T^{1.3}$ ($W \text{ cm}^{-1} \text{ K}^{-1}$).¹¹ The Stycast layer thickness forming the seal between the silicon and the CuNi tube is estimated not to exceed a few tens of microns and therefore

the cross-sectional area of the seal in contact with helium is completely negligible compared to the Si/He interface area. The influence of the Stycast layer on the heat transport across the Si/He interface is negligible as demonstrated in the Appendix. Almost all the heat in the CuNi tube is transferred along the inner surface (of area $A_{\text{CuNi,He}}$) of the tube to the superfluid He it contains. We estimated the Kapitza conductance at the CuNi/liquid He interface¹² to be $G_{\text{CuNi,He}} = 0.025T^3$ ($\text{W cm}^{-2} \text{K}^{-1}$). The conductance in the tube, over the length L , is negligible since $G_{\text{CuNi}(L)} \approx 2.4 \times 10^{-4}T^{-1.3}$ ($\text{W cm}^{-2} \text{K}^{-1}$). The conductance in the Si crystal from thermometer T_1 to the interface is $G_{\text{Si}(d)} = 0.19T^3$ ($\text{W cm}^{-2} \text{K}^{-1}$). We also took into account the Kapitza conductance¹³ from the superfluid He to the copper cell $G_{\text{Cu,He}} = 0.048T^{2.6}$ ($\text{W cm}^{-2} \text{K}^{-1}$). The $G_{\text{Cu,He}}$ can become a bottleneck at temperatures below 0.5 K depending upon the exchange area $A_{\text{Cu,He}}$. The Kapitza conductance at the Si/He interface is noted $G_K = 1/R_K$. The main equations for the heat flows are

$$\dot{Q}_o = \dot{Q}_W + \dot{Q}_I,$$

$$\dot{Q}_W = (1/G_{\text{Si,CuNi}}A_{\text{Si,CuNi}} + 1/G_{\text{CuNi}(d)}A_{\text{CuNi}} + 1/G_{\text{CuNi,He}}A_{\text{CuNi,He}})^{-1}(T_1 - T_L),$$

$$\dot{Q}_I = (1/G_K A_I + 1/G_{\text{Si}(d)}A_{\text{Si}})^{-1}(T_1 - T_L) = G_{\text{Cu,He}}(T_L - T_F).$$

We use the heater power \dot{Q}_o and set temperature T_F of the cold source during an experiment to calculate iteratively the temperature T_1 until a steady state is reached. The Kapitza conductance G_K is initially set to the values we determined from our data when assuming no heat losses, i.e., \dot{Q}_o crosses the interface. These Kapitza resistance values are determined from a differential measurement done only on thermometer T_1 . Therefore the effect of the thermal boundary (Kapitza resistance) between the thermometer T_1 and the crystal surface is annulled. The Kapitza resistance values at the Si/He interface were finally corrected after determining from our model the amount of heat really crossing the interface \dot{Q}_I and that lost to the walls \dot{Q}_W . Figure 5 shows the fraction of the input heat crossing the interface for different liquid He temperatures. Heat losses at the crystal/tube junction range from $\sim 12\%$ to less than 1% of the input power for temperatures corresponding, respectively, from 0.4 to 2 K. At temperatures lower than 0.3 K, heat losses increases rapidly and the cell configuration becomes less adapted to our experimental procedure.

In Figs. 6(a) and 6(b), the solid line fits to the temperature recordings T_1 are obtained from our model. There is clearly an overall good agreement between the fits and the measured data. However, for strong heat flux crossing the interface the fits overestimate the temperature shift of T_1 in all of our experiments [see Figs. 6(a) and 6(b)]. This is explained by nonlinearities which are introduced when the change in temperature $\delta T = (T_1 - T_L)$ becomes comparable to T_L for high heat flux. This effect is not included in our model. The correction factor can be easily found by expressing the phonon

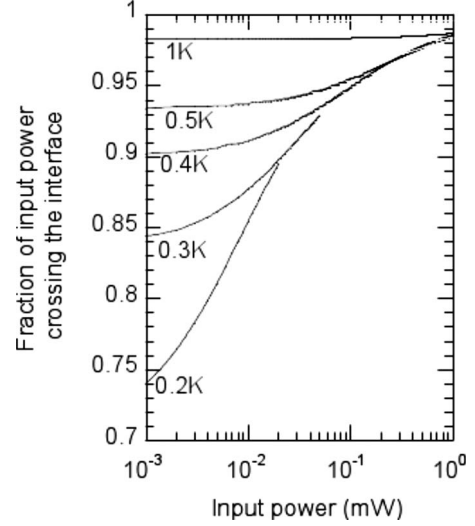


FIG. 5. Nonlinear behavior of the fraction of input heater power crossing the Si/He interface for different temperatures.

flux in the blackbody radiation picture as $\dot{q} = \alpha(T_1^4 - T_L^4)$, where α is the radiation coefficient. Substituting $T_1 = T_L + \delta T$, we get the correction to the fit of the temperature jump $\delta T' = \delta T / [1 + 1.5(\delta T/T_L) + (\delta T/T_L)^2 + 0.25(\delta T/T_L)^3]$. As an example of the importance of this effect let us consider Fig. 6(b) when 3.6 mW is supplied to the crystal. Limiting to first-order terms, we get from our measurements that $[1 + 1.5(\delta T/T_L)] \approx 1.07$ which corresponds to a correction of $\sim 6.5\%$ (~ 5.2 mK) to the associated temperature jump δT of 0.0786 K. This is in very good agreement with the difference between the fit and the measurements for this heater power in Fig. 6(b). This analysis account for all the differences between the model fit and the measured data for high heat fluxes.

For $T < 1$ K we observe an important temperature difference δT_o between T_1 and T_L in all the experiments when no heating power is supplied, i.e., $\dot{Q}_o = 0$, as seen in Figs. 2 and 6(a). Also δT_o increases as the temperatures decreases. For $T > 1$ K, δT_o is not observable [see Fig. 6(b)]. We attributed this shift to an additional residual heat flux \dot{Q}_{leak} crossing the interface. This heat flux is firstly estimated at different temperatures by expressing it as $\dot{Q}_{\text{leak}} = \delta T_o A_I / R_K$. We used the R_K values given in Fig. 7. In all of our experiments we found that the average constant value of $\dot{Q}_{\text{leak}} \approx 25$ μW for temperatures below 1 K. This estimate is in excellent agreement with a cross-check calculation of the heat flux, using the temperature gradient which is measured in the absence of \dot{Q}_o between two thermometers on the crystal and the thermal conductivity given in Fig. 3. The origin of this heat leak into the cell is most likely due to the heater wire and it limits the base temperature of the experiment.

Finally we note that the very good agreement between our thermal model and the experimental data is a strong indication of the absence of additional heat exchange surface areas (due possibly to gaps or grooves as discussed in Ref. 14). Consequently, we conclude that stray thermal boundary resistances, if present in our experimental data, are completely negligible.

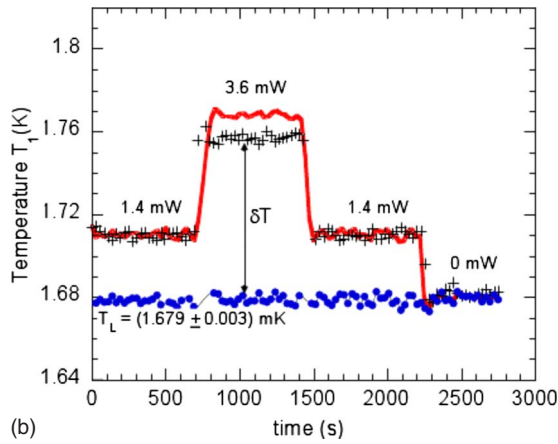
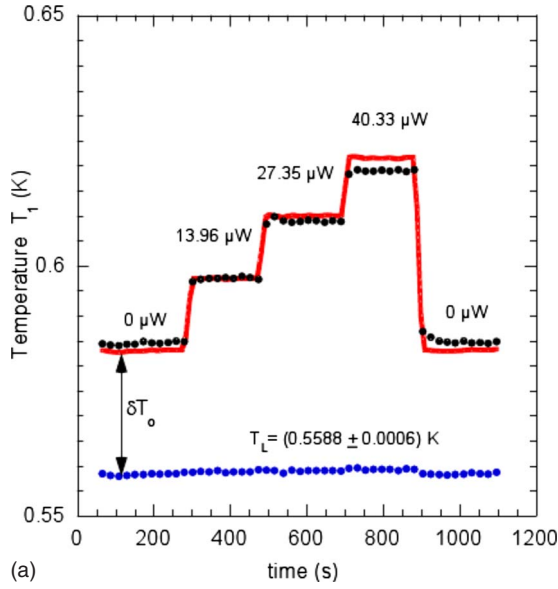


FIG. 6. (Color online) Comparison between model (solid lines) and T_1 data for (a) $T_L=0.559$ K and (b) $T_L=1.679$ K. For both cases the solid line over estimates the measured T_1 data for high input heater powers. The origin of this is explained in the text. (a) When no heat is supplied, there is a shift δT_o between T_L and T_1 as also seen in Fig. 2. (b) This shift is absent (see text).

C. Kapitza resistance at the Si/He interface

Figure 7 shows our Kapitza resistance measurements between a single-crystal Si(111) surface and liquid helium at svp pressure. Our preliminary announcement of some of this data is given in Ref. 15. The Kapitza resistance increases with decreasing temperature at different rates depending upon the temperature range. This is more clearly revealed in Fig. 8, where we plotted the transmission coefficient, determined using the expression for the Kapitza resistance¹⁶

$$R_K^{-1} = \frac{1}{4} C_p v_D \tau_\zeta. \tag{3}$$

The transmission shown in Fig. 8 is an average over all angles, all wave vectors, and all modes of phonons incident from the solid onto the interface. We now distinguish different temperature dependencies of R_K in three temperature

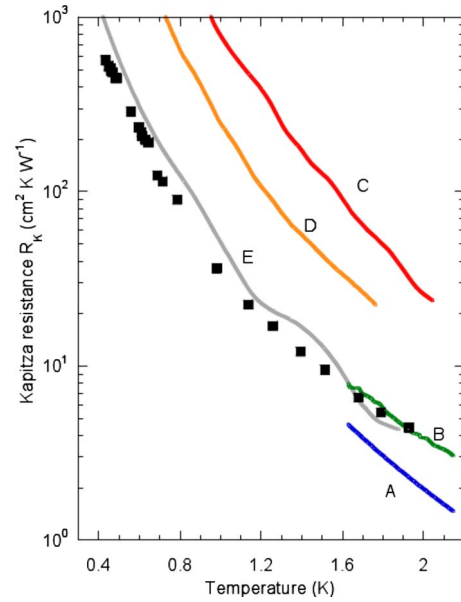


FIG. 7. (Color online) R_K as a function of T . Lines A and B represent respectively the results of Refs. 21 and 22. Lines C–E are from Ref. 17. Temperature dependencies of R_K are given in Table I.

ranges, namely: (a) $T > 1$ K, (b) $0.5 < T < 1$ K, and (c) $T < 0.5$ K. As T decreases from 2 to 1 K, R_K increases by a factor of almost four. There is a steeper increase in R_K by a factor of ~ 30 as T goes from 1 K to ~ 0.55 K [zone (b)]. For $T < 0.5$ K and down to the lowest temperature we achieved, the transmission coefficient displays an unexpected increase which implies that the R_K growth rate is hampered as T decreases. But this is not visible directly in Fig. 7. The data in Fig. 8 are well characterized by power laws given in Table I for $T > 1$ K and $T < 0.55$ K. The fit shown in Fig. 8 for $0.55 < T < 1$ K is explained later.

We recall that the AM theory predicts an average transmission of $\tau_o = 6.75 \times 10^{-3}$ [$R_K T^3 \approx 1660$ cm² K⁴/W] when heat transfer by Rayleigh waves ($F=1.6$) are taken into account. The discrepancy with our experimental data is strong in the whole temperature range, contrary to results presented

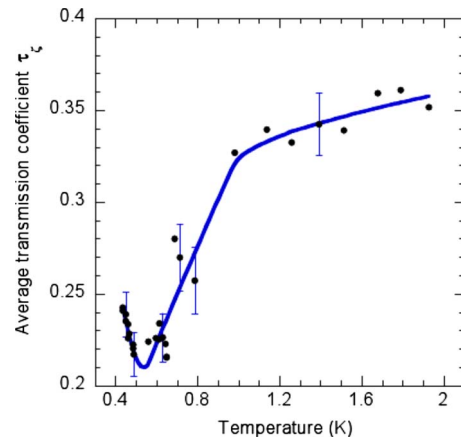


FIG. 8. (Color online) τ_ζ across the interface calculated from, our measurements, using Eq. (5). Solid line is an interpolation of the three temperature dependencies of τ_ζ .

TABLE I. Power-law temperature dependencies of σ , τ_ζ , and R_K .

	σ (nm)	τ_ζ	R_K (cm ² K W ⁻¹)
$T \gg 1$ K	$1.52T^{-0.94}$	$0.33T^{0.13}$	$34.1T^{-3.13}$
$0.5 \text{ K} < T < 1$ K	$1.51T^{-0.63}$	$0.32T^{0.74}$	$34.4T^{-3.74}$
$0.5 \text{ K} < T$	$0.90T^{-1.44}$	$0.12T^{-0.89}$	$97.0T^{-2.11}$

in Ref. 17 as we shall see later. This is clear evident that diffuse phonon scattering, whatever its origin, is therefore predominant. Thus we conclude that the components of wave vector parallel to the interface plane are not conserved even at temperatures as low as 0.4 K on our crystal surface which is smooth to within less than a nanometer on the scale of a micron.

D. Scattering of phonons at a rough surface

To interpret our average transmission shown in Fig. 8 we shall consider the AF model. In this model, phonons are incident from liquid He onto the surface. In summary, the AF model derives the amplitude of the reflected Φ_1 transmitted wave Φ_2 using appropriate boundary conditions and as a function z which is the value of the surface vertical-height profile $\zeta(r)$ at a point r in the xy plane. To ensure a proper statistical description of the surface roughness the autocorrelation function of the surface is defined as $\langle \zeta(r)\zeta(r+\rho) \rangle = \sigma^2 e^{-(\rho/\delta)^2}$, where σ is the root-mean-square surface roughness height. The Gaussian distribution is a crucial assumption and it accounts reasonably well for the isotropic nature of σ at a given scale length. The enhancement of the energy flux (which is proportional to $|\Phi_2|^2$) carried across the interface is characterized by a scattering amplification function $f(\delta/\lambda)$ which is temperature dependent. The average normalized transmission coefficient is found to have the following behavior:

$$\frac{\tau_\zeta}{\tau_o} = \left(1 + \frac{1}{2} \gamma^2 f(\delta/\lambda) \right), \quad (4)$$

where τ_o is the transmission coefficient for an ideal surface as given by the AM theory and $\gamma = 2\sigma/\delta$ is a typical roughness inclination which relates σ to δ .

Under the constraint $\delta \approx \sigma < \lambda$, the AF model shows that $f = 169(\delta/\lambda)^2$, where the numerical coefficient is due to elastic constants. We emphasize the point that there are no other corrective higher order terms in (δ/λ) . When $(\delta/\lambda) \approx 0.5$ the model predicts that scattering of phonon by surface roughness becomes strongly diffusive and phonons outside the critical cone, as defined by the AM theory, contribute to heat flux which constitutes the background channel.

In our case we chose our crystal surface to be mirrorlike such that on a scale length of λ the model requirement $\delta \approx \sigma < \lambda$ is satisfied. Consequently, we simplify the average transmission coefficient given in Eq. (4), after neglecting the first term, as

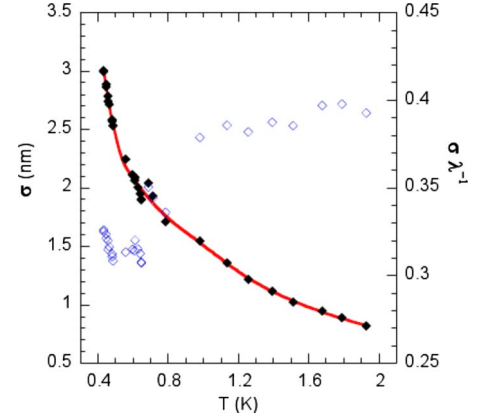


FIG. 9. (Color online) σ versus T (full diamonds) determined from Eq. (5). Solid line corresponds to the temperature dependencies in Table I. Ratio of (σ/λ) as a function of T (open diamonds).

$$\tau_\zeta \approx 2.16(\sigma/\lambda)^2 = 0.14(\sigma T)^2, \quad (5)$$

where σ is expressed in nm and T in Kelvin. Here we took the dominant phonon wavelength $\lambda(\text{nm}) \approx 4/T$.

Using Eq. (5), we plot in Fig. 9 the surface roughness values σ extracted from our experimental transmission data. Interesting features are revealed. Firstly, the σ values which suffice to explain the increased heat transmission in the whole temperature range lies between ~ 0.7 and ~ 3 nm. Characterization of our crystal surface confirms the presence of roughness of these values. The surface roughness of our polished Si(111) sample is characterized using two different techniques, namely, atomic force microscopy (AFM) and optical microscopy (OM). The root-mean-square roughness σ values measured with these techniques are displayed in Fig. 10. The diamonds (\diamond) in Fig. 10 are obtained after analysis of OM images, using a surface mapping software (Phase Shift Technology, Inc.®). Each (\diamond) at a given scale length in Fig. 10 is an average over 250 data points which were obtained within scan areas of a few μm^2 . FFT analysis of OM images at different scale lengths indicates clearly a Gaussian-

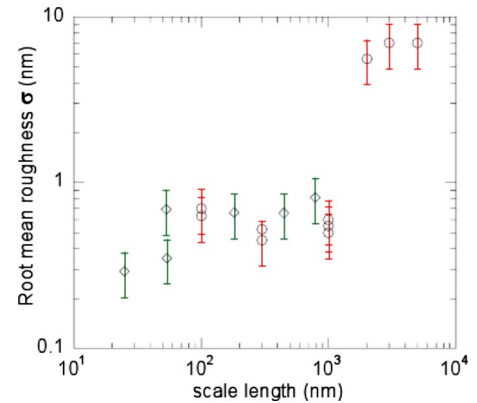


FIG. 10. (Color online) Root-mean-square roughness σ of the Si(111) surface at different scale lengths. The diamonds and the circles correspond, respectively, to measurements performed by optical microscopy and by AFM. For scale lengths less than 10^3 nm, $\sigma \lesssim 1$ nm.

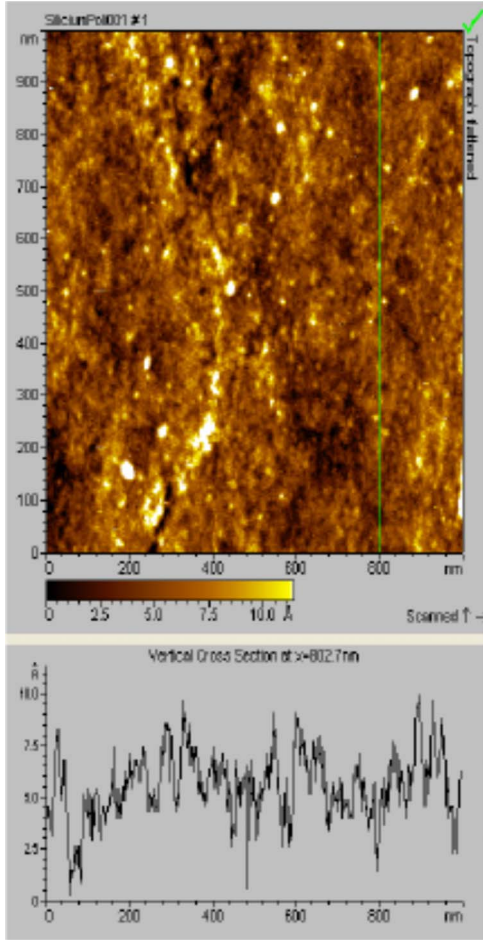


FIG. 11. (Color online) Typical AFM image ($1 \mu\text{m}^2$) of the Si(111) surface and surface roughness profile (in \AA).

like distribution of σ values associated with that scale length. The full circles in Fig. 10 are AFM measurements, obtained in the tapping mode. Figure 11, which is a typical topographical AFM image conducted over a scan area of $1 \mu\text{m} \times 1 \mu\text{m}$, shows also that there is a distribution of σ values present on our sample surface.

Secondly, as seen in Fig. 9, $\sigma \propto 1/T^n$ where $n \geq 0$. In Fig. 9 we show also the ratio (σ/λ) , which increases from ~ 0.3 to ~ 0.4 for T ranging from 0.4 to 2 K. The experimental outcome $\sigma < \lambda$ is in agreement with the model requirement. Also, the orders of magnitude of (σ/λ) are in excellent agreement with the AF model prediction for the scattering to be diffuse and/or resonant. The fact that (σ/λ) ratio undergoes a relatively small change suggests that there is a preferential selection of σ , which is determined by the thermal phonon wavelength, such that the momentum transfer is optimal at the interface. Further, we deduce that the increased phonon momentum transfer at the interface requires the condition $|\vec{k}\delta| \approx 2.2$ to be satisfied, where k is the incident wave vector. We also remark that a larger density of roughness height σ of increasing size is required as the temperature decreases. The lack of surface roughness comparable in size to the wavelengths at low temperatures (see Fig. 10) may explain the small decrease in (σ/λ) observed at $T < 1$ K.

In view of the above discussion it is now clear that transmission coefficient is entirely controlled by the phonon-

surface roughness interaction and its temperature dependency. The temperature dependencies of σ , shown in Table I for three different temperature ranges, account quantitatively for the observed R_K . The fit to the data in Fig. 8 for $0.5 < T < 1$ K is obtained from the power law describing σ . The solid line fits in Figs. 8 and 9 are interpolations of the temperature dependencies given in Table I. The T dependency of σ discovered here implies that the effective heat exchange area at a microscopic scale depends on the thermal frequency of phonons. We found that this interesting feature, which emerges naturally in our analysis, was evoked by Little¹⁸ in the literature. Little argued in Ref. 18 that the smaller the wavelength, the greater the effective area A_λ available for heat exchange. Hence, he predicted that A_λ was to increase with increasing phonon energy (frequency ω) as $A_\lambda = A_o \omega^n$, where A_o is the nominal macroscopic area and $n > 0$ when $(\sigma/\lambda) \gg 1$. Little’s formulation is valid only in the limit of high frequencies since, as $\omega \rightarrow 0$, we must have $A_\lambda \rightarrow A_o$. Writing the increase in the effective exposed area as $(A_\lambda/A_o) \approx 1 + 2(\sigma/\lambda)^2$, we have that heat transport across the interface will be greater than the AM theory predication when $(\sigma/\lambda) \gg 1$. In the present work, as shown in Fig. 9 and supported by the characterization of our sample surface in Fig. 10, we have $0.3 < (\sigma/\lambda) < 0.4$, and consequently the effective area A_λ differs very little from A_o in the whole temperature range of the experiment. The enhanced heat transfer through the surface, even at shorter wavelengths, is therefore not due to an increase in the effective exchange area. The diffuse or resonant scattering process privileges phonon interactions with certain roughness heights among the Gaussian distribution present on the surface, as discussed above. Thus σ increases with the wavelength λ of phonons as in Fig. 9. Since $A_\lambda \propto \sigma^2$, we expect A_λ to increase (at a microscopic scale) with decreasing phonon frequency. We point out that the arguments here are valid only when $\sigma < \lambda$.

For the sake of completeness, we note that Little also studied¹⁹ the effect of the interaction between microscopic roughness and phonons of comparable wavelengths on heat flow. For this case, his model indicates that the Kapitza resistance at solid/liquid helium interfaces is slightly greater for microscopically rough surfaces than for ideally smooth surfaces given by the AM theory. This predication has never been observed experimentally.

In our analysis we have taken the dominant heat transfer process to be due to the phonon-surface roughness interaction leading to diffuse scattering of phonons. The σ values shown in Fig. 9 must therefore correspond to upper limit values. We might expect slight modifications in these values in the event of parallel heat transfer mechanisms. Nevertheless, the fundamental conclusions of our analysis remain unchanged.

Finally, we make three observations. Firstly, our experiment is conducted with helium having a ^3He impurity concentration of $\sim 2 \times 10^{-7}$. As demonstrated by Duncan *et al.*²⁰ and corroborated by Murphy and Meyer,¹⁴ the effects of this concentration level are not detectable on R_K unless the temperatures are within 10^{-3} of the λ point. Secondly, additional thermal boundary resistance due to the suppression of the superfluid counterflow in a “skin” layer of liquid in contact

with the solid is not present in our experiment. As discussed also by Duncan *et al.*²⁰ this effect, which exists even when ^4He is ultra pure, manifests itself only at temperatures within 10^{-3} of the λ point. Thirdly, the superfluid correlation length varies over our experimental temperature range but remains always much smaller than any characteristic phonon wavelength or surface roughness scale of the Si surface. It was therefore not considered in our analysis.

E. Comparison with other studies

We next compare our results to previous studies on Si. The only other direct Kapitza resistance measurements^{21,22} on silicon/liquid helium interfaces were conducted at temperatures higher than 1.4 K and are shown by curves (A) (Ref. 21) and (B) (Ref. 22) in Fig. 7. Curve (A) represents measurements conducted by Johnson *et al.* on Si(111) [$R_K = 35T^{-4.15}$ cm² K/W]. The crystallographic orientations with respect to the direction of the heat flux in the present work and in that of Johnson *et al.* are the same. Further, it is generally accepted that at least the first layer of He in contact with the Si substrate has a solidlike structure. The hcp crystalline symmetry of Si [111] surface matches that of solid ^4He (which has also an hcp structure). As seen from Fig. 7, the R_K values of these two experiments agree within a factor of two. Little is known about the surface state of their samples. Discrepancies of these orders of magnitude were found in other studies,²³ in the same temperature range, which focused on the impact of systematic surface treatments (chemical etching or electropolishing) leading to different surface roughness on a micron scale for a given sample.

Figure 7 also shows that curve (B) representing our previous measurements on Si(001) [$R_K = 46.2T^{-3.58}$ cm² K/W] at $T > 1.5$ K and the present work are very consistent. The experimental configurations are very different in both cases. Both samples have highly polished surfaces of roughness of the order of $\lesssim 2$ nm at scale lengths $\lesssim 1$ μm . The good agreement between this work (Si [111]) and curve (B) (Si [001]) suggests that the influence of surface roughness primes over probable effects due of the crystallographic orientation in phonon transmission at $T > 1$ K. It would be interesting to examine this aspect for $T < 1$ K.

In Fig. 7, curves C–E represent the data of Olson and Pohl¹⁷ obtained on 0.3-mm-thick Si(111) wafers. Curves C, D, and E correspond, respectively, to a clean Syton polished Si surface, a Si surface covered with an amorphous SiO_2 film of 2160 Å thickness and a plasma etched Si surface. The study of Olson and Pohl is conducted between 2 and 0.05 K, a wider temperature range than the one covered in the present investigation. We note that their R_K data are determined rather indirectly from their thermal conductivity measurements performed on these samples when covered with liquid ^4He . Using their estimates of the mean free path l_p , they calculated by Monte Carlo simulations the transmission coefficient α_{diff} and the probability f for phonons to undergo diffuse scattering at the Si/He interface. Defining the total average phonon transmission coefficient for $T > 0.3$ K as $\alpha \equiv \alpha_{diff}f$ and with the aid of Eq. (3), they determined R_K as shown in Fig. 7. Firstly, we note that the discrepancy be-

tween our results and that represented by curve C increases from a factor of ~ 10 at $T \sim 2$ K to a factor of ~ 70 at $T \sim 0.4$ K. These discrepancies are reduced by a factor of two when comparing our results with sample D. Our sample certainly has oxide layers—but differences in the results of samples C and D become negligible at $T \lesssim 0.3$ K, where they found R_K for these samples to approach the value predicted by the acoustic mismatch theory. We note that these discrepancies with our results are puzzling since samples C, D, and ours are polished mirrorlike surfaces, having similar surface roughness. Further, there is a relatively good agreement between the Olson and Pohl measurements of l_p of phonons in sample C ($l_p \sim 0.8$ cm) compared to our value ($l_p \sim 0.52$ cm) (Sec. III B). Sample D has a $l_p \sim 1$ cm. Secondly, the agreement between our measurements and results of sample E, shown in Fig. 7, is also puzzling. This is so because the plasma-etched Si surface (curve E) has a “black-velvet-like¹⁷” appearance with bumps which were ~ 0.3 μm in diameter and height. Further, sample E has a $l_p \sim 10$ cm, which is a factor of ~ 20 larger than our value. AFM analysis of our sample surface shows that at scale lengths of the order of 1 μm , our sample surface roughness has an average value of $\lesssim 1$ nm.

We remark also that at $T \approx 0.3$ K the R_K values of Olson and Pohl¹⁷ for samples C and D reach the acoustic mismatch prediction.²⁴ Our present data extrapolated to 0.3 K do not attain the AM theory prediction since the effect of phonon scattering by surface roughness remains preponderant. From Eq. (5), we have that an almost complete suppression of diffuse scattering requires $(\sigma/\lambda) \lesssim 0.0056$. For this condition to be met at $T = 0.3$ K, the mean surface roughness $\sigma \lesssim 0.75$ Å at scale lengths greater than 13 nm, which is an extremely stringent condition to be met especially on sample D which has an amorphous SiO_2 layer. It is also interesting to note that Olson and Pohl found for all three samples that $0.3 < \alpha_{diff} \leq 1$ for $0.3 < T < 2$ K, which demonstrates that roughness comparable in size to the liquid phonon wavelength must also be present on their Syton-polished surface. This corroborates the importance of the diffuse scattering mechanism as we have shown in our experiment. Consequently, it appears as if the discrepancies in the results shown in Fig. 7 are due to the small values of the factor f describing the probability of diffuse scattering to occur, which depends on the geometry of their sample.

Finally we note that our average transmission coefficient compares well to those measured in experiments using the heat-pulse technique²⁵ and, in particular, with the measurements performed by Guo and Maris²⁶ in phonon reflection studies on a Si(111) polished sample covered with liquid He films of ~ 10 Å at 1.85 K. (see Fig. 7 in Ref. 26).

IV. CONCLUDING REMARKS

We have conducted TCR measurements at a Si/ ^4He interface that spans the temperature range 0.4 to 2.1 K using a single cell. The chemical purity of the crystal surface remained unchanged throughout the experiment. The results constitute the first set of data for a highly polished dielectric

material in a sufficiently wide temperature range so that the temperature dependence of TCR can be studied. Based on the Adamenko and Fuks model, we have demonstrated the importance of surface roughness in the transmission of phonons at liquid ^4He /surface boundaries. We have quantified the degree of surface roughness which comes into play in comparison with the thermal wavelength of phonons of liquid ^4He . We have also put to evidence a feature which is the temperature dependency of the surface roughness height σ . The latter reveals to be a key parameter to quantitatively account for the temperature dependency (exponent) of R_K ; and it has to be included in future models.

Finally, we note that the sensitivity of σ on T suggests that R_K can prove to be a useful probe of surface roughness at nanoscale. This present investigation shall also serve a more general purpose of understanding thermal contact resistance in thermal management studies of microstructured and nanostructured systems, where the underlying physics is also determined by phonon scattering at boundaries or interfaces.²⁷

ACKNOWLEDGMENTS

I acknowledge the CNRS for funding my stay in the R & D Low Temperature group at the IPNO where this experiment was carried out. I thank P. Bujard, F. Chatelet, F. Dubois, Q. Li, and J. P. Thermeau for helping in setting up the experiment; and M. Ammar for taking part of the AFM images. My sincere thanks go to J. C. Poulin and M. Lancry of the ICMNO for helping with the surface characterization. I also wish to acknowledge a fruitful exchange with T. Nakayama a few years ago and with A. F. G. Wyatt. I thank B. Castaing for discussions.

APPENDIX

We analyze here heat flow through the Stycast seal between the CuNi tube and the Si crystal, and we show that its influence on our R_K measurements at the Si/He interface is negligible. We consider an extreme case where the all heat loss \dot{Q}_{Sty} from the Si to the Stycast, over an area of $A_{\text{Si,Sty}} = A_{\text{Si,CuNi}} \propto l \approx 2.2$ mm, is transported along the Stycast layer only and across the Stycast/He interface. The Stycast bond layer is estimated (by measuring the diameter of the crystal and that of the tube) to be ~ 25 μm thick. We determine \dot{Q}_{Sty} by modifying the previous model used to calculate heat losses to the CuNi tube (see Sec. III B).

We define the conductance $G_{\text{Si,Sty}}$ as the Kapitza conductance from the Si crystal to the Stycast epoxy. We estimate $G_{\text{Si,Sty}}$ as we did for the CuNi/Si interface. We compute the longitudinal (L) and transverse (T) transmission coefficients from Si to the Stycast epoxy to be, respectively, $\tilde{\alpha}'_L = 0.647$ and $\tilde{\alpha}'_T = 0.604$, with the following values for Stycast 2852FT epoxy: $\rho_{\text{Sty}} = 2.1$ g/cm³, $c'_L = 2.5 \times 10^5$ cm/s, and $c'_T = 1.8 \times 10^5$ cm/s. The longitudinal and transverse velocities (c'_L and c'_T) are typical values for epoxies. For Si we used the values given previously. The conductance turns out to be $G_{\text{Si,Sty}} = 0.0128T^3$ (W cm⁻² K⁻¹). Knowing the thermal conductivity of Stycast 2852 FT at 1 K (Ref. 8) and using the

fact that an amorphous material generally shows a T^2 behavior in its thermal conductivity²⁸ at low temperatures, we take the thermal conductivity of Stycast to be $K_{\text{Sty}} \approx 6.5 \times 10^{-5}T^2$ (W cm⁻¹ K⁻¹) for $T < 2.1$ K. The conductance in the Stycast layer is therefore $G_{\text{Sty}(l)} = (K_{\text{Sty}}/l) \approx 3 \times 10^{-4}T^2$ (W cm⁻² K⁻¹). The Kapitza conductance $G_{\text{Sty,He}}$ between the epoxy and liquid He is poorly documented in the literature. We shall take this conductance to be infinite. Clearly, a finite value of $G_{\text{Sty,He}}$ can only lead to a smaller \dot{Q}_{Sty} . Also, this assumption overcomes the problem of determining the effective surface exchange area $A_{\text{Sty,He}}$ between the Stycast and liquid He due to an eventual formation of a meniscus of the epoxy. However, the Stycast epoxy seal was examined by eye and it did not show a meniscus. Also, upon drying the Stycast epoxy has a shiny black smooth surface.

The main equations of for heat flow are now

$$\dot{Q}_o = \dot{Q}_{\text{Sty}} + \dot{Q}'_I,$$

$$\begin{aligned} \dot{Q}_{\text{Sty}} = & (1/G_{\text{Si,Sty}}A_{\text{Si,Sty}} + 1/G_{\text{Sty}(l)}A_{\text{Sty}} \\ & + 1/G_{\text{Sty,He}}A_{\text{Sty,He}})^{-1}(T'_1 - T_L), \end{aligned}$$

$$\dot{Q}'_I = (1/G_K A_I + 1/G_{\text{Si}(d)}A_{\text{Si}})^{-1}(T'_1 - T_L),$$

where A_{Sty} and A_{Si} are, respectively, the cross-sectional surface areas of the Stycast and the Si crystal.

The model calculations show that $\dot{Q}_{\text{Sty}} \lesssim 0.2\%$ of the input heat \dot{Q}_o in the whole temperature range of this experiment. A heat leak through the Stycast bond is completely negligible. This outcome is not surprising since $G_{\text{Sty}(l)}A_{\text{Sty}} \ll G_{\text{CuNi}(d)}A_{\text{CuNi}} \ll G_{\text{Si}(d)}A_{\text{Si}}$. We also note that $A_{\text{Sty}}/A_{\text{Si}} \approx 1.6\%$ and $A_{\text{Sty}}/A_{\text{CuNi}} \approx 12.5\%$.

Finally, we make three remarks. Firstly, our value of $G_{\text{Si,Sty}}$, which is calculated using the AM theory, is in fact overestimated. Studies of the Kapitza resistance between solid/epoxy interfaces by Matsumoto *et al.*²⁹ show that at $T > 0.2$ K, the epoxy acts as a ‘‘low pass filter’’ in a sense that the epoxy reduces the transport of high frequency ($> 10^{11}$ Hz) thermal phonons across the interface (see Fig. 2 in Ref. 29). The Kapitza resistance between solid/epoxy interfaces turn out to be greater than the AM theory predictions for $T > 0.2$ K. We also note that the thicknesses of the epoxies examined in Ref. 29 are similar to that in present study.

Secondly, we estimate $(G_{\text{Sty,CuNi}}/G_{\text{Si,Sty}}) \approx 50$, where $G_{\text{Sty,CuNi}}$ is the conductance from the Stycast to the CuNi tube wall. Heat is more easily transmitted from the Stycast layer to the CuNi tube wall than it is carried along the Stycast layer.

Thirdly, when considering heat loss the from the Si crystal to the CuNi tube we supposed an ideal interface between the CuNi tube and the Si crystal. As we have shown, the presence of the Stycast bond makes the CuNi/Si interface ‘‘less’’ ideal and leads to an increase in the thermal resistance between the CuNi tube and the Si, compared to the estimated ideal value. Our calculations of the heat losses to the CuNi tube walls (in Sec. III B) therefore represent an upper limit.

- ¹T. Nakayama, in *Progress in Low Temperature Physics*, edited by D. F. Brewer (North Holland, Amsterdam, 1989), Vol. XII, Chap. 3, p. 115.
- ²E. T. Swartz and R. O. Pohl, *Rev. Mod. Phys.* **61**, 605 (1989).
- ³A. F. G. Wyatt, in *Nonequilibrium Superconductivity, Phonons, and Kapitza Boundaries*, edited by K. E. Gray (Plenum Press, New York, 1981), Vol. 65, Chap. 2.
- ⁴I. M. Khalatnikov, *Introduction to the Theory of Superfluidity* (Benjamin, New York, 1965), Chap. 23.
- ⁵J. Weber, W. Sandmann, W. Dietsche, and H. Kinder, *Phys. Rev. Lett.* **40**, 1469 (1978).
- ⁶N. S. Shiren, *Phys. Rev. Lett.* **47**, 1466 (1981); H. Kinder, *Physica B (Amsterdam)* **107**, 549 (1981); T. Nakayama, *Phys. Rev. B* **33**, 8664 (1986).
- ⁷I. N. Adamenko and I. M. Fuks, *Zh. Eksp. Teor. Fiz.* **59**, 2071 (1970) [*Sov. Phys. JETP* **32**, 1123 (1971)].
- ⁸LakeShore data sheet available on their website.
- ⁹T. Klitsner and R. O. Pohl, *Phys. Rev. B* **36**, 6551 (1987).
- ¹⁰J. D. N. Cheeke, B. Hebral, and C. Martinon, *J. Phys. (France)* **34**, 257 (1973).
- ¹¹H. A. Fairbank and D. M. Lee, *Rev. Sci. Instrum.* **31**, 660 (1960).
- ¹²We used the values of Kapitza resistance between CuNi/⁴He given by L. Puech, Ph.D thesis, Université Joseph Fourier, Grenoble, France, 1983.
- ¹³K. Wey-Yen, *Zh. Eksp. Teor. Fiz* **42**, 921 (1962) [*Sov. Phys. JETP* **15**, 635 (1962)].
- ¹⁴D. Murphy and H. Meyer, *J. Low Temp. Phys.* **99**, 745 (1995); **105**, 185 (1996); **107**, 175 (1997).
- ¹⁵J. Amrit and J. P. Thermeau, *J. Phys. Conf. Ser.* **150**, 032002 (2009).
- ¹⁶L. J. Challis, *J. Phys. C* **7**, 481 (1974).
- ¹⁷J. R. Olson and R. O. Pohl, *J. Low Temp. Phys.* **94**, 539 (1994).
- ¹⁸W. A. Little, *Can. J. Phys.* **37** (3), 334 (1959).
- ¹⁹W. A. Little, *Phys. Rev.* **123**, 1909 (1961).
- ²⁰R. V. Duncan, G. Ahlers, and V. Steinberg, *Phys. Rev. Lett.* **58**, 377 (1987).
- ²¹R. C. Johnson and W. A. Little, *Phys. Rev.* **130**, 596 (1963).
- ²²J. Amrit and M. X. Francois, *J. Low Temp. Phys.* **128**, 113 (2002).
- ²³J. Amrit and M. X. François, *J. Low Temp. Phys.* **119**, 27 (2000).
- ²⁴Thus far $R_K \propto T^{-3}$ has been observed only on experiments conducted on solid/liquid ³He interfaces at $T \leq 0.3$ K. This is explained by the onset of zero-sound modes in liquid ³He at these temperatures; see also J. Amrit and J. Bossy, *Europhys. Lett.* **15**, 441 (1991).
- ²⁵J. Wolter and R. E. Horstman, *Phys. Lett. A* **61**, 238 (1977).
- ²⁶C. J. Guo and H. J. Maris, *Phys. Rev. Lett.* **29**, 855 (1972).
- ²⁷R. J. Stoner and H. J. Maris, *Phys. Rev. B* **48**, 16373 (1993); P. G. Murphy and J. E. Moore, *ibid.* **76**, 155313 (2007).
- ²⁸R. O. Pohl, X. Liu, and E. Thompson, *Rev. Mod. Phys.* **74**, 991 (2002); J. R. Olson, *Cryogenics* **33**, 729 (1993).
- ²⁹D. S. Matsumoto, C. L. Reynolds, Jr., and A. C. Anderson, *Phys. Rev. B* **16**, 3303 (1977).